Yeast TATA Binding Protein Interaction with DNA: Fluorescence Determination of Oligomeric State, Equilibrium Binding, On-Rate, and Dissociation Kinetics†

Gina M. Perez-Howard, P. Anthony Weil, and Joseph M. Beechem*

Department of Molecular Physiology and Biophysics, Vanderbilt University School of Medicine, Nashville, Tennessee 37232-0615

Received March 8, 1995®

ABSTRACT: A combination of steady-state, stopped-flow, and time-resolved fluorescence of intrinsic tryptophan and extrinsically labeled fluorescent DNA is utilized to examine the interaction of yeast TATA binding protein (TBP) with DNA. TBP is composed of two structural domains, the carboxy domain (residues 61−240), which is responsible for DNA binding and initiation of basal level transcription, and an amino terminal domain (residues 1−60), whose function is currently unknown. The steady-state fluorescence emission spectrum of the single tryptophan in the amino terminal domain of TBP undergoes a huge (30−40 nm) red-shift upon interaction with stoichiometric amounts of TATA box containing DNA. From time-resolved tryptophan fluorescence anisotropy studies, we demonstrate that, in the absence of DNA, the protein exists as a multimer in solution and it contains (at least) two primary conformations, one with the amino terminus associated tightly with the protein(s) in a hydrophobic environment and one with the amino terminus decoupled away from the rest of the protein and solvent-exposed. Upon binding DNA, the protein dissociates into a monomeric complex, upon which only the solvent-exposed amino terminus conformation remains. Kinetic and equilibrium binding studies were performed on TATA box containing DNA which was extrinsically labeled with a fluorescent probe Rhodamine-X at the 5′-end. This "fluorescent" DNA allowed for the collection of quantitative spectroscopic binding, kinetic on-rate, and kinetic off-rate data at physiological concentrations. Global analysis of equilibrium binding studies performed from 500 pM to 50 nM DNA reveals a single dissociation constant (K_d) of approximately 5 nM. Global analysis of stopped-flow anisotropy on-rate experiments, with millisecond timing resolution and TBP concentrations ranging from 20 to 600 nM (20 nM DNA), can be perfectly described by a single second-order rate constant of 1.66×10^5 M^{-1} s^{-1}. These measurements represent the very first stopped-flow anisotropy study of a protein/DNA interaction. Stopped-flow anisotropy off-rate experiments reveal a single exponential k_{off} of 4.3×10^{-2} min^{-1} ($1/k_{off} = 23$ min). From the ratio of on-rate to off-rate, a predicted K_d of 4.3 nM is obtained, revealing that the kinetic and equilibrium studies are internally consistent. Deletion of the amino terminal domain of TBP decreases the k_{on} of TBP approximately 45-fold and eliminates classic second-order behavior.

The TATA binding protein (TBP) is a DNA binding protein that interacts with the TATA box element (consensus sequence TATAAAA) (Hernandez, 1993). In eucaryotes, TBP is the core protein subunit of RNA polymerase II general transcription factor TFIID, a multiprotein complex consisting of TBP and TBP-associated factors (TAFs) (Dynlacht et al., 1991; Pugh & Tijan, 1992; Tijan & Maniatis, 1994). The TBP subunit of TFIID is absolutely required to initiate gene transcription (Nakajima et al., 1988; Cavallini et al., 1989; Hahn et al., 1989a,b; Horikoshi et al., 1989a,b; Schmidt et al., 1989). It directs the TFIID, and ultimately the ordered assembly of other proteins at the promoter, by binding to the TATA box with high affinity, thus leading to formation of a functional preinitiation complex (Zawel & Reinberg, 1993). Although TBP was initially thought to be required for the transcription of just RNA polymerase II genes, it has additionally been found to be required for the transcription of RNA polymerase I and III genes (for a recent review, see Hernandez, 1993).

Recently, the crystal structure of yeast and plant TBP (Chasman et al., 1993; Nikolov et al., 1992) and cocrystal structures of these same two TBPs with TATA box DNA have been solved (Kim, J., et al., 1993; Kim, Y., et al., 1993). In all of the crystal structures which have been solved, the amino terminal part of TBP was either lacking or had been removed; therefore, this part of the TBP structure is unknown. The structure of carboxy terminal domain of TBP in the presence and absence of DNA has a "saddle-like" shape whose "underneath" is formed from antiparallel β strands. When the crystal structure of TBP was originally determined, it was hypothesized that the DNA would "fit" directly into this saddle region. However, when the cocrystal structure was actually solved, a much more interesting TBP/DNA structure was observed. In this structure, the DNA strands approach the TBP saddle at a very oblique angle (≈22°). The DNA strands then undergo a radical "kink" and slightly separate from each other, with one DNA strand passing along the "front" of the saddle region, and the other strand passing along the "back" along the minor groove of the DNA. The minor groove becomes almost completely "flattened", and the DNA bends toward the major groove side. The DNA then exits at the other end of the saddle and undergoes another sharp "kink" upon exiting TBP.

† J.M.B. was supported by the Lucille P. Markey Charitable Trust and S10 RR05823. P.A.W. was supported by NIH Grants GM52461 and GM40517.

® Abstract published in *Advance ACS Abstracts,* June 1, 1995.

0006-2960/95/0434-8005$09.00/0

Examination of the crystal structure of TBP in the presence and absence of DNA reveals that surprisingly little structural change is induced in the carboxy terminal domain of TBP upon interaction with DNA. The experiments described in this report were designed to probe the kinetics and equilibrium properties of the TBP−DNA binding reaction, and values for these kinetic and thermodynamic parameters were determined. During the course of these studies, we found that a very large change in the amino terminal domain of TBP occurs upon interaction with DNA.

Saccharomyces cerevisiae yeast TATA binding protein (TBP) is a 27 kDa protein comprised of 240 amino acid residues. Yeast TBP contains a single tryptophan residue which is located in the amino terminal region (W26) (Horikoshi et al., 1989a,b) of the protein. Two distinct structural domains of TBP have been genetically and biochemically defined. The carboxy terminal region (≈residues 60−240) has been shown to be absolutely required for DNA binding and basal level transcription in vitro (Horikoshi et al., 1990; Lieberman et al., 1991) and in vivo (Cormack et al., 1991; Gill & Tijan, 1991; Poon et al., 1991; Reddy & Hahn, 1991; Zhou et al., 1991; Kelleher et al., 1992). The carboxy terminal domain region of TBP appears to contain the core of TBP's functionality, and its sequence is highly conserved between species (see Hernandez, 1993). In contrast, the amino terminal sequence of TBP is not conserved among species, being highly variable in both length and sequence, and its exact role in the transcriptional process is unknown. There have been several genetic studies on TBP where the amino terminal domain has been removed. In vitro analyses of these genetically altered forms of TBP have shown that amino terminally deleted forms of TBP exhibit enhanced DNA binding activity (Horikoshi et al., 1990; Lieberman et al., 1990). Also, Lieberman et al. (1990) has shown that a temperature dependent property exists for the TBP−DNA binding and that removal of the amino terminal domain relaxes this temperature dependence. Both Lee et al. (1992) and Kuddus and Schmidt (1993) have suggested a possible role for the amino terminus of TBP in regulating DNA binding activity of the C-terminal domain since, upon its removal, it (a) affects the overall stability of the TBP−DNA complex, (b) affects the ability of non-DNA binding mutant forms of TBP to bind DNA efficiently (Lee et al., 1992), and (c) caused TBP to interact with all TAFs without discrimination (Zhou & Berk, 1995).

Experiments were undertaken in order to determine if the single tryptophan residue (W26) located in the center of the amino terminal domain would be sensitive to possible changes in structure and dynamics which might occur in TBP upon interaction with duplex TATA box containing DNA. Tryptophan fluorescence has proven to be a very useful spectroscopic marker for major state transitions in proteins for many different systems (Beechem & Brand, 1985 and references therein). With this in mind, both steady-state and time-resolved fluorescence techniques were utilized to examine TBP's interaction with DNA. From these measurements, information concerning the oligomeric state of the native TBP and the changes in the rotational dynamics of the amino terminal domain of TBP upon binding DNA was determined.

Tryptophan fluorescence spectroscopy lacks the inherent sensitivity to perform equilibrium binding and kinetic experiments at physiological concentrations for the majority of specific protein/DNA interactions (picomolar to nanomolar). To circumvent this drawback, a fluorescently labeled TATA box containing DNA was synthesized. This extrinsically labeled DNA was utilized to determine the kinetic and equilibrium binding properties of TBP to DNA. Anisotropy studies of TBP/DNA interaction can be performed in a thermodynamically rigorous manner, without the inherent limitations and assumptions associated with gel-shift type binding assays, which are by necessity performed under nonequilibrium conditions. Data densities and timing resolution are also greatly extended, compared to more classical molecular biological assays of equilibrium binding and kinetics. This increased data density and timing resolution also allow more rigorous types of data analysis. Simultaneous global nonlinear fitting of concentration dependent equilibrium and kinetic experiments is performed. Using these two fluorescence-based approaches, intrinsic tryptophan fluorescence and extrinsically labeled DNA fluorescence, quantitative examination of the interaction of TBP with DNA is possible.

MATERIALS AND METHODS

Purification of Recombinant TBP. The TBP purification procedure utilized is described in Horikoshi et al. (1989a,b) with modifications as described by in Poon et al. (1993). After passing the *Escherichia coli* cell extract through a heparin−Sepharose column, the resin was washed with LB/200 buffer (20 mM Tris-HCl, pH 7.9, 10% glycerol, plus 20 mM 2-mercaptoethanol, 1 mM phenylmethanesulfonyl fluoride (PMSF), and 200 mM NaCl). The bound protein was batch eluted with LB buffer containing 1000 mM NaCl. TBP was further purified using ion exchange chromotography on a Mono-S FPLC column (Pharmacia). Protein was loaded onto the Mono-S column at 100 mM NaCl in LB buffer and eluted with a linear, 10 column volume gradient of NaCl (100−1000 mM) in LB buffer. The final salt concentration in the TBP pooled fractions generated via Mono-S chromatography was about 500 mM NaCl, and the protein concentration was estimated to be approximately 0.2 mg/mL. The purity of this TBP preparation was estimated by analysis of silver-stained SDS−PAGE to be greater than 99% (i.e., no other bands could be visualized). Absolute protein concentrations were determined using amino acid analysis on a Waters Pico-tag system.

Oligonucleotide Synthesis. Most binding studies, utilizing protein tryptophan emission, were performed with synthetic oligonucleotides of varying length (14, 16, 18, and 41 bp) which are derivatives of the TATA box sequence of the adenovirus major late promoter:

5′-GCGTATAAAATGCG-3′

5′-GGCGTATAAAATGCGG-3′

5′-GCGGCTATAAAATGGCGG-3′

5′-GTTCCTGAACGGCGGCTATAAAATGG-
CGGTGGCGGCGCGTG-3′

For nontarget DNA studies, the TATA box (underlined above) was replaced with the sequence GCGGCCGC. Oligonucleotide syntheses were performed on a Cyclone 8400 Plus DNA synthesizer (Milligen/Biosearch, Burlington, MA).

Steady-state anisotropy equilibrium binding and kinetics measurements used a fluorophore-labeled synthetic oligomer with the sequence GGGCTATAAAAGGG*R* (where *R* represents Rhodamine-X isothiocyanate; R-491 Molecular Probes, Eugene, OR) attached via a 5′ amino linker (5′-Amino-Modifier C6, Glen Research, Sterling, VA). In order to successfully obtain labeled oligo that is stable and pure, the following procedure was developed. To initially label with the isothiocyanate fluorophore derivatives, the oligo was dissolved in a solution of 0.1 M sodium bicarbonate, pH 9.0. The fluorophore derivative was dissolved in dimethylformamide (DMF) to a final concentration of 10 mg/mL. The fluorophore solution was added dropwise to the oligo with mixing, and the solution was covered and incubated overnight at 30 °C. Free fluorophore was removed by gel filtration chromatography (Bio-Gel P-6 DG, Bio-Rad, Richmond, CA), eluting with 10 mM Tris, 0.1 mM (or 1 mM) EDTA, pH = 7.9 (T.1E, TE, respectively). DNA-containing fractions were identified by absorbance at 260 nm, pooled, and concentrated by ethanol precipitation. At this point, in order to remove any nonlabeled $(n-1)$mer species and residual free fluorophore, the modified DNA was electrophoresed on a denaturing 15% polyacrylamide−urea electrophoresis gel (13 cm × 8 mm × 80 cm, gel cast in 89 mM Tris, 89 mM boric acid, 2 mM EDTA, and 8 M urea, and run in the same buffer without urea). The gel was preelectrophoresed for 1 h at a constant power of 80 W. Labeled oligos were resuspended in a denaturing sample buffer (5 M urea, 0.05% xylene cyanol, 0.05% bromophenol blue, 50 mM sodium hydroxide, and 1 mM EDTA) to a final volume of 50 μL, denatured by heating at 95 °C for 3 min, and loaded onto the gel, and the gel was run for 8−12 h. The purified fluorophore-labeled oligos were visualized with UV light (2 nm), excised from the gel, and extracted from the gel pieces by diffusion into elution buffer (T.1E, 0.05% SDS, 50 mM NaCl) by incubation overnight in a 65 °C water bath. The solution was concentrated with 2-butanol to a final volume of 500 μL and extracted once with a mixture of phenol/chloroform with isoamyl alcohol (1:1:pH 8.0, AMRESCO, Solon, OH), twice with chloroform alone, and once with ether. DNA was then precipitated with 2 volumes of cold absolute EtOH, containing 10 mM $MgCl_2$ at −20 °C overnight. DNA was recovered by centrifugation, and the labeled oligo was dissolved in TE. The DNA concentration was quantified at both A_{556} and at A_{260}. The A_{260} molar extinction coefficient was calculated for each sequence-specific strand using software developed from the measured pairwise base extinction interaction data reported by Fasman (1975). The labeled oligo was annealed with an equimolar amount of its complementary strand in TE containing 200 mM NaCl by denaturation at 100 °C for 3 min in a water bath followed by slow cooling overnight. Duplex fluorophore-labeled oligos were gel purified on a 20% native polyacrylamide electrophoresis gel in order to separate the nonannealed single strands from the duplex. This combination of initial purification of the labeled single strands on ultralarge sequencing type gels followed by separation of duplex from single stranded DNA after annealing ensures 100% labeled duplex DNA was utilized in our studies. Since the Rhodamine-X probe exhibits such a strong fluorescence emission, we could monitor the TBP/DNA interaction with very high signal to noise at very low protein and DNA concentrations (picomolar to nanomolar range).

Proteolysis of TBP. Limited proteolysis of TBP was performed as described by Lieberman et al. (1991). Briefly, 4 μL of a stock solution of 0.22 mg/mL chymotrypsin (Sigma Chemicals, St. Louis, MO), in 10% glycerol, 20 mM HEPES (pH 7.9), and 1 mM EDTA, was added to 165 μL of a 0.08 mg/mL TBP protein solution. The sample was incubated at room temperature (~23 °C) for 60 min, and proteolysis was terminated by the addition of 0.1 mM final concentration PMSF.

TBP Binding Conditions. Unless otherwise stated, all binding and kinetics experiments are performed under the following conditions: 7% glycerol, 100 mM NaCl, 7 mM $Mg^{2+}Cl_2$, and 20 mM HEPES, pH = 7.9, 20 ± 2 °C. In all experiments where the final TBP concentrations were less than 100 nM, 50−100 μg/mL bovine serum albumin (BSA fraction V; Sigma) was added in order to prevent nonspecific absorption of TBP or probe to glass, plastic surfaces, and the interior lines of the stopped-flow unit.

Fluorescence Measurements. Fluorescence measurements were performed utilizing either a laser or xenon-arc light source. The xenon-arc light source was composed of a 75-W Oriel (Stratford, CT) lamp coupled to a 1/4 meter monochromator and high-grade fused silica optical fiber. Excitation wavelength for this system was 295 nm (5 nm bandpass). The laser system was composed of a frequency doubled Coherent Antares Nd:YAG laser (Palo Alto, CA) synchronously pumping a dual dye-jet (Coherent 702) laser using Rhodamine 6G and a DODCI saturable absorber. Output pulses from this laser at both 293 and 295 nm were utilized at 4 MHz and had a pulse width of approximately 1 ps. Steady-state fluorescence detection was performed with a Princeton Instruments (Princeton, NJ) optical multichannel analyzer (OMA, Model IPDA-512 G/B, ST1000 controller) coupled to an Instruments SA (Edison, NJ) 1/3 meter polychromator with fiber optic input from a 100 μL cuvette (Helma Corp., Jamaica, NY). Time-resolved fluorescence experiments utilize time-correlated single photon counting with two types of detection setups. The principal detection optics were the same as for steady-state experiments, except the OMA was replaced with a Hamamatsu 10 linear anode two-stage intensified 12 μm microchannel plate (Bridgewater, NJ, Model R3839U-07). Detection electronics involved a parallel set of high frequency 50× amplifiers (Phillips Scientific 774, Mahwah, NJ), constant fraction discriminators (Tennelec 454, Oak Ridge, TN), time-to-amplitude converters (Tennelec 862), and pulse-height analysis analog to digital converters (Nucleus PCA-II, Oak Ridge, TN). Time-resolved fluorescence anisotropy experiments were performed using a single channel 6 μm Hamamatsu (R2809U-01, Bridgewater, NJ) microchannel plate detector. The collimated fluorescence emission passed through Glan-Thompson polarizers on automated mounts in an ISS KOALA (Urbana, IL) sample compartment and then was focused onto the entrance slits of a SPEX (Edison, NJ) 0.22 m emission monochromater. The emission polarizer was rotated between parallel and perpendicular polarizations every 30 s, and the data were averaged over 30−60 min of collection. This system was also utilized for equilibrium binding titrations performed at low protein and DNA concentrations. For these experiments, the emission polarizer was rotated every 15 s and a software-selectable region of the parallel and perpendicular integrals (selected so as to time-resolve away the scattered light contribution) was

obtained. A running average of 10−40 anisotropy determinations were obtained for each titration point, and the measured standard deviations of the recovered data were used to weight the nonlinear fitting of the data. For total-intensity experiments collected between 310 and 340 nm, real-time backgrounds were collected in parallel with the protein fluorescence so as to account for the Rayleigh and Raman scattering.

Global Analysis of Equilibrium and Kinetic Data. Equilibrium binding isotherms were fit to the following equation (Weber, 1993):

$$r_m = [fx_b]r_b + [fx_f]r_f$$

where:

$$fx_b = \frac{1}{2}\left(1 + \frac{k_d}{[DNA]} + \frac{[TBP]}{[DNA]}\right) \times \left\{1 - \left[1 - \left(4\frac{[TBP]}{[DNA]}\right)\Big/\left(1 + \frac{k_d}{[DNA]} + \frac{[TBP]}{[DNA]}\right)^2\right]^{1/2}\right\}$$

[TBP] and [DNA] are the total protein and DNA concentrations, k_d is the dissociation constant for the TBP−DNA complex, fx_f and fx_b represent the fractional population of the free and bound DNA, and r_b and r_f represent the steady-state anisotropies of the bound and free DNA, respectively (there is no quantum yield change in this system, so the direct fractions can be utilized; see Otto et al., 1994).

Stopped-flow on-rate experiments were directly fit to the finite differential equations describing the reaction:

$$[TBP{-}DNA(t+\Delta t)] = [TBP{-}DNA(t)] + k_{on}[TBP(t)][DNA(t)]\Delta t - k_{off}[TBP{-}DNA(t)]\Delta t$$

where [TBP−DNA] and [DNA] are the instantaneous concentrations (time = t) of the TBP−DNA bound complex and free DNA, respectively. Integration is performed using a Δt of 5−50 ms, depending on the timing resolution of the experiment. The measured stopped-flow anisotropy can be calculated from these populations using:

$$r_m(t+\Delta t) = [fx_b(t+\Delta t)]r_b + [fx_f(t+\Delta t)]r_f$$

where fx_b, fx_f, r_b, and r_f are as described above. These equations were inserted into the general purpose Globals Unlimited nonlinear fitting routines (Urbana, IL; Beechem et al., 1992), allowing all multiconcentration stopped-flow experiments to be simultaneously analyzed in terms of a single second-order rate constant.

Time-Resolved Fluorescence Data Analysis. Time-resolved total intensity data collected at multiple emission wavelengths were analyzed using global nonlinear least-squares analysis techniques (e.g., Beechem, 1992; Beechem et al., 1992).

For the time-resolved anisotropy data, the intensities parallel and perpendicular to the excitation wavelength were simultaneously analyzed in terms of

$$3I_{\parallel}(t) = [\sum_{i=1}^{nt}\alpha_i \exp(-t/\tau_i)][1 + 2\sum_{j=1}^{nr}\beta_j \exp(-t/\varphi_j)]\otimes Ex(t)$$

$$3I_{\perp}(t) = [\sum_{i=1}^{nt}\alpha_i \exp(-t/\tau_i)][1 - \sum_{j=1}^{nr}\beta_j \exp(-t/\varphi_j)]\otimes Ex(t)$$

where nt and nr denote the total number of total intensity lifetimes and rotational correlation times, respectively, ⊗ is the convolution operator, and $Ex(t)$ is the measured instrument response function. Rigorous confidence interval analysis for all of the data described in this work is performed as described in Beechem (1992). Fluorescence steady-state emission center of mass (ν) calculations were performed as follows:

$$\nu(\lambda_i) = \frac{\sum_i F(\lambda_i)\,\lambda_i}{\sum_i F(\lambda_i)}$$

where $F(\lambda_i)$ represents the steady-state emission measured at emission wavelength i. Decay associated spectra were calculated using the method of Wahl (Brochon et al., 1977), with values for the recovered lifetimes coming from a global simultaneous nonlinear analysis of all emission wavelength dependent kinetics:

$$DAS(\lambda_i) = \frac{\alpha_i(\lambda_i)\,\tau_i}{\sum_{i=1}^{nt}\alpha_i(\lambda_i)\,\tau_i}F(\lambda_i)$$

Stopped-Flow Fluorescence Detection. Reactions were performed with an SFM-3 stopped-flow unit (Molecular Kinetics, Pullman, WA) with a 50 μL FC.15 fluorescence cuvette and hard-stop shutter essentially as described in Otto et al. (1994). Reaction flow rates were 4 mL/s. Reaction time bases were typically 50 ms per channel, and data were collected in 8000 total channels. Stock solutions of TBP, dilution buffer, and TATA box DNA were loaded into separate syringes. For all experiments, solutions were extensively degassed. All experiments were collected with a fraction of the data channels devoted to internal controls. Tryptophan total-intensity stopped-flow experiments were performed using stock solutions of TBP and TATA box DNA at concentrations of 438 and 700 nM, respectively. Excitation wavelength was 295 nm (±4 nm) using a SPEX 450-W xenon arc lamp and 0.22 m monochromator coupled to a fused silica optical fiber. Emission was detected through a 340-nm cut-on filter (Hoya L34), and fluorescence photon counting multichannel scaling counting was performed (Tennelec MCS2; Oak Ridge, TN). Rhodamine-X-labeled DNA stopped-flow anisotropy experiments (T-format) were performed using 580 nm (±2 nm) excitation at a concentration of 20 nM. TBP concentrations were adjusted to range from 20 to 600 nM. All mixing was performed at a 1:1 ratio, using 200 μL total volume per reaction. Fluorescence emission was detected using 600 nm cut-on filters (Hoya, R60) [see Otto et al. (1994) for additional details]. All reactions (unless specifically noted) were performed at 20 ± 2 °C. Multiple (10−15) kinetic runs were summed to obtain adequate signal to noise ratios.

RESULTS

The changes in the steady-state emission spectrum of the single tryptophan in wild-type (WT) TBP as a function of DNA concentration are shown in Figure 1. In the absence of DNA, TBP has a very blue-shifted emission (≈320 nm peak). Upon binding of TBP to DNA, a very large red-shift occurs in the emission spectra, changing the maximum

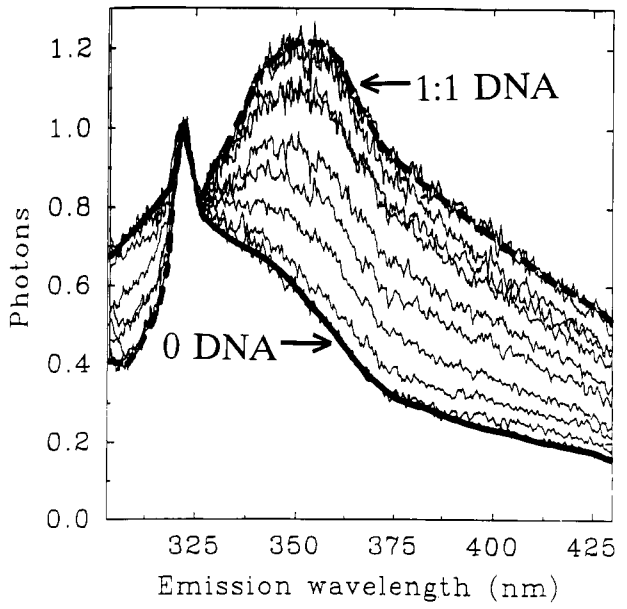

FIGURE 1: Effect of TATA-DNA addition upon the fluorescence emission spectra of TBP. The mole ratio of DNA/TBP ranged from 0 (solid line) to 1 (dashed line) as shown. Excitation wavelength = 293 nm, emission collected in 512 elements of an optical multichannel analyzer at approximately 0.25 nm/element. All spectra are normalized to the water Raman peak at 323 nm.

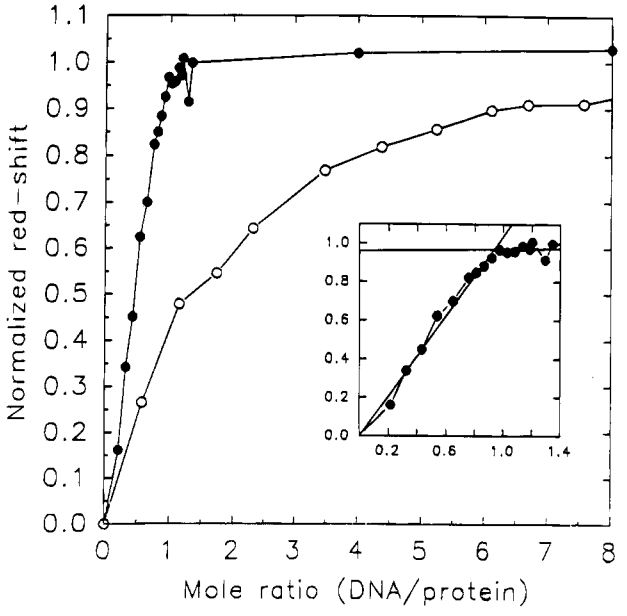

FIGURE 2: Stoichiometric binding isotherms for the interaction of TBP with TATA and non-TATA DNA using W26 tryptophan fluorescence red-shift. Excitation and emission settings same as in Figure 1; the normalized red-shift represents the center of mass calculation given in text. The protein concentration was 2 μM; (●) DNA which contains TATA box, (○) DNA with no TATA box (see Materials and Methods). Inset shows an expanded view of the TBP−TATA binding profile with a stoichiometric breakpoint of approximately 0.95. Protein concentration was determined by amino acid analysis.

to ≈353 nm. In order to verify that the red shift of the emission spectra was actually due to the binding of TBP to DNA, titration experiments were performed (Figure 2). Plotting the center of mass of the emission peak versus the mole ratio of DNA/TBP reveals a stoichiometric binding profile, with saturation at 1 mol of DNA/mol of TBP. Figure 2 also shows the binding of TBP to nontarget DNA, where the TATA box has been replaced with a series of

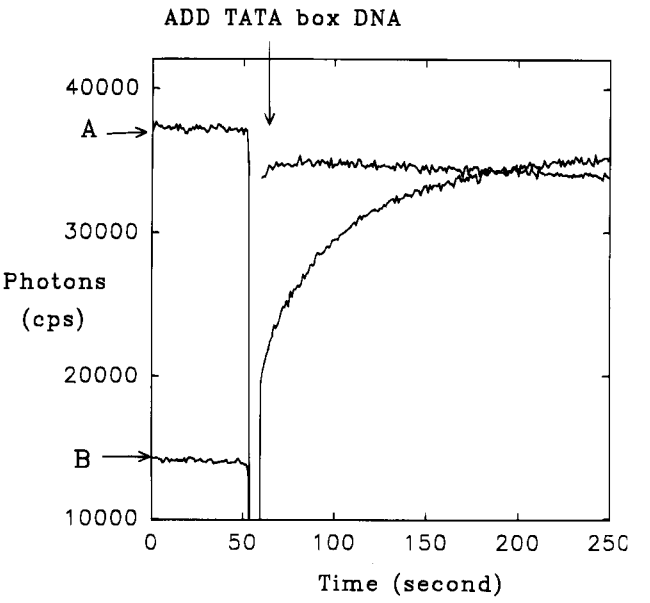

FIGURE 3: Dual color real-time kinetics of TBP binding to DNA at 4 °C. TBP excitation was 295 nm. The fluorescence emission was observed simultaneously at 310 nm (A; decreasing amplitude signal) and 370 nm (B, increasing amplitude signal) as a function of time. At this low temperature spectral changes were found to occur over an extended period of time (hours). Only the initial phase of the reaction is shown in this figure.

cytosines/guanines (see Materials and Methods). A dramatic red-shift is observed for this nonspecific binding, but the affinity of TBP for the nontarget DNA has decreased significantly.

Previous kinetic studies have revealed that the TBP/DNA interaction is relatively slow kinetically, especially at low temperatures (Hoopes et al., 1992). To further prove that the spectral changes depicted in Figures 1 and 2 are directly related to DNA binding, the observed spectral shift in the tryptophan fluorescence was examined kinetically at 4 °C using simple "hand-mixing" to initiate the binding reaction. Figure 3 illustrates a dual-color binding kinetics profile, where TBP tryptophan fluorescence emission is monitored simultaneously at 310 and 370 nm. These data clearly reveal the relatively slow kinetics associated with the observed red-shift. A full kinetic study of this interaction will be presented below. Tryptophan spectral shifts of the magnitude observed here (30−40 nm) are usually found only when proteins undergo total unfolding. We examined the effects of TBP denaturation upon the spectral properties of the TBP tryptophan. Shown in Figures 4 and 5 are the observed spectral shifts in TBP when TBP is denatured with guanidine or elevated temperature. In both cases, the emission spectra evolve from the very blue-shifted emission to a red-shifted emission with a peak at 353 nm, spectra which are identical to the TBP−DNA bound emission spectra. The temperature dependent unfolding of TBP revealed two phases with midpoints centered at 30 and 42 °C. It is interesting to note that addition of stoichiometric amounts of DNA can induce spectral changes in the tryptophan emission similar to those for increasing temperature and the presence of denaturants. Control experiments (mixing TBP with buffer, repeated scans, etc.) resulted in no change in the emission spectral center of mass.

Time-resolved anisotropy experiments were performed on free TBP and TBP−DNA complexes in order to further

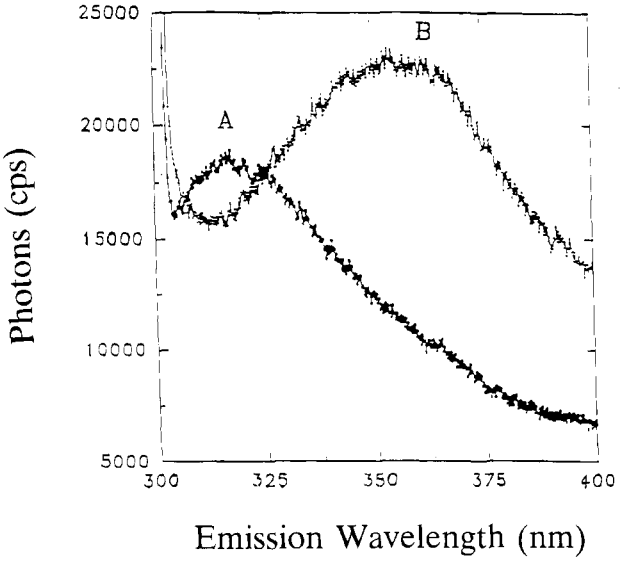

FIGURE 4: Effect of guanidine hydrochloride upon the fluorescence emission spectrum of TBP. Fluorescence emission spectra of TBP were collected in the presence of either 0.0 M (A) or 1.37 M (B) GuHCl. Full concentration dependent scans (data not shown) yielded a midpoint of the GuHCl induced denaturation of TBP to be 1.0 M. Other conditions were the same as in Figure 2.

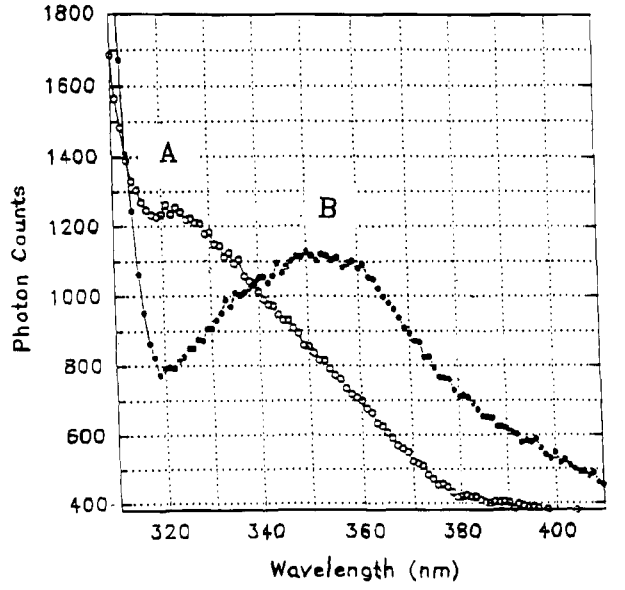

FIGURE 5: Effect of temperature upon the steady-state emission spectra of TBP. Spectra were collected either at 4 °C (A) or at 52 °C (B). Full temperature dependent scans (data not shown) yielded midpoints of the thermal denaturation to be 30.5 and 42 °C. Excitation = 295 nm, excitation/emission bandpass = 8 nm.

investigate the origin of the large spectral shift induced by DNA binding. If the amino terminus of TBP is tightly coupled to the carboxy (i.e., the DNA binding) domain, an increase in the overall rotational correlation time of the protein–DNA complex should be observed relative to TBP alone. The rotational correlation time predicted for a spherical complex of 27 kDa (TBP's molecular mass) is approximately 12 ns (allowing 50% hydration). Upon binding of TBP to the 41mer TATA-DNA, the molecular mass of the bound complex should double to approximately 54 kDa. A TBP–DNA 41mer complex would be predicted to exhibit a rotational correlation time of approximately 24 ns. Time-resolved anisotropy decays of the 350 nm tryptophan emission of the free, bound, and protease-digested

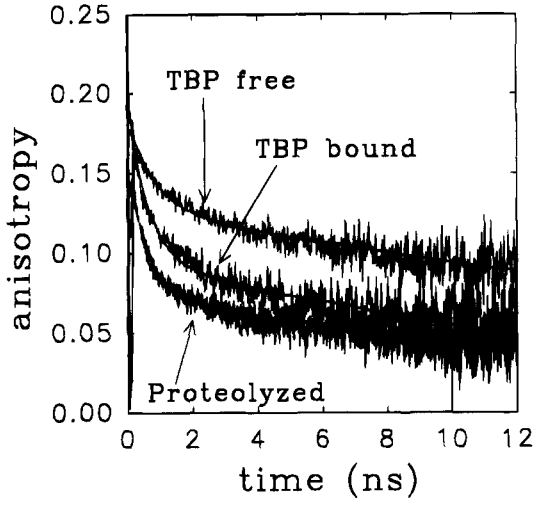

FIGURE 6: Time-resolved anisotropy utilizing the endogenous W26 fluorophore of WT TBP. Time-resolved anisotropy of (top curve) native TBP, (middle curve) TATA box containing DNA bound to TBP, and (bottom curve) protease-treated TBP and protease-treated TBP–DNA complex (both curves superimpose). Timing calibration was 6 ps per channel. Data contained approximately 20 000–50 000 counts at the peak of the vertically polarized decay curve.

TBP are shown in Figure 6. In the absence of DNA, the anisotropy decay curve of native TBP is best fit with two rotational correlation times, a minor fast component of 1.7 ns and a major slow component which is emission wavelength dependent (described below). Surprisingly, upon addition of stoichiometric amounts of TATA-DNA, instead of the predicted increase in the rotational correlation times, their values actually decrease (see Figure 6).

A particularly sensitive protease cleavage site exists between the carboxy region and amino terminus end of the protein (at amino acid 40). Cleaveage of TBP with proteases allows the examination of the rotational correlation time of the isolated amino terminal domain of TBP, which contains the reporting tryptophan residue W26. The anisotropy decay of the protease-treated TBP is also shown in Figure 6. Identical anisotropies are obtained when proteolysis is performed on prebound TBP–DNA complexes, or when free TBP is proteolyzed.

Since the expected increase in rotational correlation time for the TBP–DNA complex was not observed using TBP's intrinsic tryptophan fluorophore, experiments were conducted using fluorescently labeled TATA box DNA. This change in procedure allows the binding process to be monitored from the DNA perspective, independent of complex transitions which may be occurring in the amino terminus of TBP. Time-resolved anisotropy measurements taken on Rhodamine-X-labeled DNA alone and Rhodamine-X-labeled DNA complexed with TBP are shown in Figure 7 (upper). The rotational correlation time for Rhodamine-X-labeled 14mer DNA is dominated by a 6.7 ns rotation along with a small amplitude fast motion term. The calculated "spin" and "tumble" times for the 14mer duplex DNA are 4.4 and 9.85 ns, respectively (Tirado & de la Torre, 1980), indicating that the measured rotational correlation time of 6.7 ns probably represents an average of these two rotational modes. Upon binding TBP, the rotational correlation time for the protein–DNA complex increases to 17 ns. These experimental results indicate that, from the perspective of the DNA, the TBP–DNA complex indeed rotates more slowly than naked DNA.

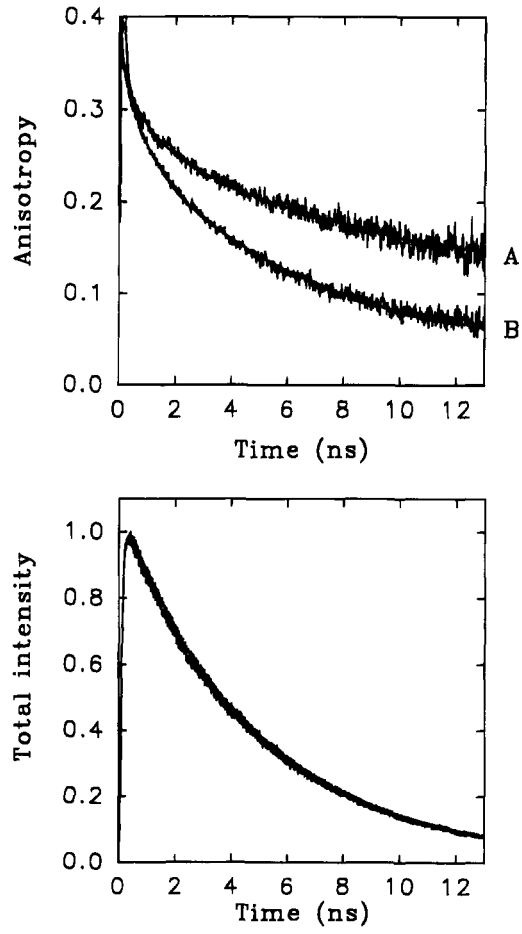

FIGURE 7: Time-resolved measurements of TBP/DNA interaction with extrinsically labeled Rhodamine-X DNA. Time-resolved anisotropy of Rhodamine-X labeled DNA alone (upper panel, B) at 62 nM concentration, and bound with saturable amounts of TBP (upper panel, A). Time-resolved total intensity decays of the Rhodamine-X DNA (lower panel) in the absence and presence of TBP are plotted, and both are superimposable, revealing essentially no change in the fluorophore lifetime when TBP binds DNA.

Figure 7 (lower) illustrates the time-resolved total-intensity decays of the probe. These plots reveal that there is no change in the lifetime of the DNA probe upon binding with the protein, indicating that the observed signal changes are only associated with changes in the rotational mobility of the DNA.

Since nanomolar/picomolar concentration ranges of extrinsically labeled DNA can be monitored, nonstoichiometric equilibrium binding titrations can be performed with these reagents. This allowed us to make direct spectroscopic determinations of the dissociation constant (K_d) of TBP for TATA box DNA. Since the TBP/TATA interaction exhibits very complex behavior when monitored using the gel-shift assay (Hoopes et al., 1992), these equilibrium binding titrations should provide a new and independent evaluation of the K_d for TBP. TBP/DNA binding isotherms (Figure 8) were obtained at DNA concentrations ranging from 0.89 to 10 nM. The steady-state anisotropy value of the free DNA is 0.14, while the TBP-DNA complex reaches an anisotropy asymptote of approximately 0.23. When the measured anisotropies are plotted on a TBP/DNA mole ratio axis, the binding isotherms should shift to higher and higher mole ratios due to mass action effects; this was found to be the case (Figure 8). Global analyses of all three binding isotherms in terms of a single internally consistent K_d were performed, and a single K_d of 5 nM was determined from the analyses.

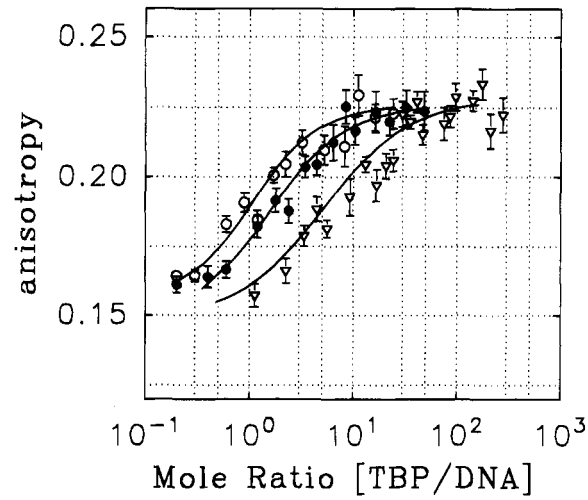

FIGURE 8: Measurement of the equilibrium K_d of the TBP–TATA complex via changes in the anisotropy of the Rhodamine-X DNA 14mer. Equilibrium binding titrations of TBP with Rhodamine-X-labeled DNA at DNA concentrations of 10 nM (○), 5 nM (●), and 890 pM (▽). Linked global analysis across the various DNA concentrations (smooth line fits) was performed in terms of a single K_d, yielding 5 nM; see Table 1.

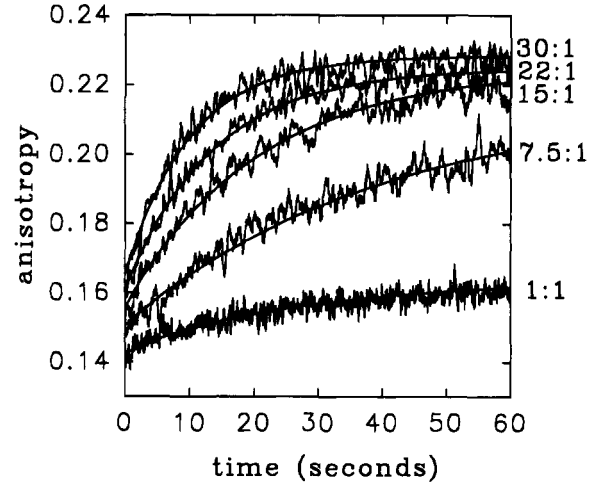

FIGURE 9: Measurement of the kinetics of binding of TBP to Rhodamine-labeled TATA box DNA using stopped-flow anisotropy. Stopped-flow on-rate kinetics measurements were performed using 20 nM TATA 14mer fluorescent DNA and the following concentrations of TBP (bottom to top): 20, 150, 300, and 600 nM. Time scale for the 1:1 binding kinetics curve is compressed by 10 times in order to fully view this slower rise (i.e., full-scale maximum is 600 s). Global simultaneous analysis of the stopped-flow anisotropy data (smooth line fit through all of the data) was performed in terms of a single internally consistent second-order rate constant (k_{on}). These data sets can be very well described using only a single k_{on} of 1.66×10^5 M^{-1} s^{-1}.

One of the tremendous advantages of using fluorescence anisotropy to monitor TBP/DNA binding is that real-time binding kinetics can be examined. These data were obtained by conducting stopped-flow anisotropy experiments using 20 nM Rhodamine-X-labeled DNA and varying mole ratios of TBP to DNA, ranging from 1:1 to 30:1 (see Figure 9). The time required for TBP to bind the TATA-DNA ranges from less than 30 s at a 30:1 mole ratio to greater than 18 min at 1:1. Global simultaneous analysis of the stopped-flow anisotropy data over this entire concentration range was performed in terms of a single internally consistent second-

Table 1: Kinetic and Equilibrium Characterization of WT and ΔN TBP

TBP	k_{on} (M^{-1} s^{-1})	$1/k_{off}$ (min)	K_{eq} (from kinetics)	K_{eq} (data)
wild type	$1.66 \times 10^{+5}$ (+0.14) (−0.03)	23 (+1.5) (−1.6)	4.3 nM (±0.2)	5 nM (+3) (−1)
ΔN	$3.6 \times 10^{+3}$	nd	nd	nd

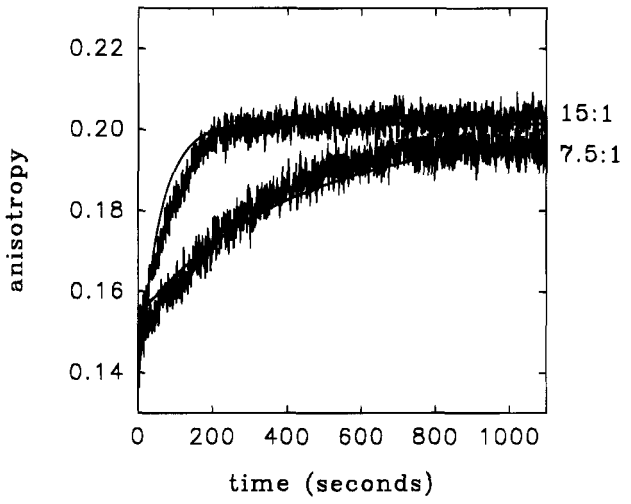

FIGURE 10: Measurement of the kinetics of binding of ΔN TBP to Rhodamine-X-labeled TATA box DNA using stopped-flow anisotropy. Stopped-flow on-rate kinetics measurements were performed using 20 nM TATA 14mer DNA and ΔN TBP at either 150 or 300 nM. Global simultaneous analysis of the stopped-flow anisotropy data (smooth line fit through all of the data) was performed in terms of a single internally consistent second-order rate constant (k_{on}). These data sets do not appear to follow simple second-order reaction kinetics. The "mean" second-order rate constant recovered from this analysis (smooth line fit to the data) is k_{on} of 3.6×10^3 M^{-1} s^{-1}, approximately 45 times slower than WT TBP (compare with Figure 9).

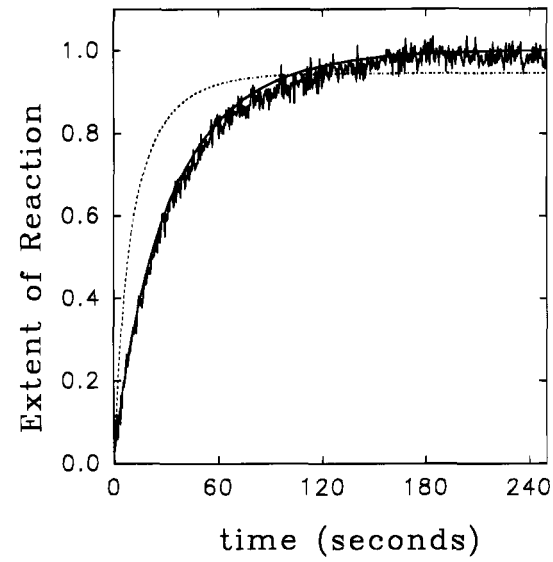

FIGURE 11: Kinetics of binding of TBP to TATA-DNA by monitoring the endogenous TBP tryptophan fluorophore. Real-time binding kinetics and smooth fit curve of 438 nM WT TBP binding to 700 nM 14mer DNA (not labeled with Rhodamine-X) using the increase in tryptophan total intensity observed >340 nm as a measure of the extent of binding. A second-order rate constant of 3.6×10^3 M^{-1} s^{-1} is obtained from the analysis. The dashed line represents the predicted kinetic trace which would have been observed using the second-order rate constant measured by Rhodamine-X fluorescence anisotropy (Table 1).

order rate constant (k_{on}). As shown in Figure 9, one can see that all of these data sets can be very well described using only a single k_{on} of 1.66×10^5 M^{-1} s^{-1} (see Table 1). Stopped-flow on-rate binding kinetics of an amino terminal deleted form of TBP (ΔN TBP) were also measured. The on-rate kinetics at both 7.5:1 and 15:1 molar excess of protein/DNA is shown in Figure 10. Direct comparison of these data with Figure 9 reveals that the binding of ΔN TBP to TATA-DNA is much slower than WT TBP. Global analysis of these data in terms of a single second-order rate constant reveals that the simple binding pattern of WT TBP is not maintained. The second-order rate constant which is obtained from this analysis is approximately 45 times slower than that of WT TBP (see Table 1). A detailed study of this mutant will be described in a future publication (Perez-Howard et al., 1995; in preparation).

Stopped-flow on-rate experiments were also performed utilizing the large red-shift in the tryptophan fluorescence. While it is not possible to span exactly the same concentration range as the Rhodamine-X on-rate kinetics due to limited sensitivity, very good signal to noise can be obtained when analyzing TBP concentrations as low as 438 nM. Measurement of the kinetics of TBP binding to TATA-DNA, utilizing the increase in fluorescence intensity at wavelengths greater than 340 nm (i.e., the kinetics of the red-shift described shown in Figures 1 and 2), is shown in Figure 11. The second-order rate constant obtained from this data set is 3.66×10^4 M^{-1} s^{-1}, a value significantly lower than that obtained from the Rhodamine-X study (see Figure 9 and Table 1). A possible origin for this difference in k_{on} is described in the Discussion.

Off-rate experiments can also conveniently be performed using stopped-flow anisotropy techniques. For these experiments, TBP was prebound to the Rhodamine-X-labeled DNA, yielding a steady-state anisotropy value of 0.23. This prebound complex was then rapidly mixed with an excess of unlabeled (i.e., nonfluorescent) TATA box containing DNA, and the decrease in anisotropy as a function of time was measured. An example of this type of assay is shown in Figure 12. For experiments performed at relatively low initial TBP/DNA concentrations (e.g., <8:1), the off-rate of TBP from the DNA can be described using a single time constant ($1/k_{off}$) of 23 min (see Table 1).

Having completely defined the equilibrium and kinetic properties of TBP/DNA interaction, studies were initiated to further understand the origin of the large tryptophan fluorescence emission spectral shift in TBP upon interaction with DNA. Time-resolved total-intensity and anisotropy measurements were performed on free and bound TBP as a function of emission wavelength. We found that the time-resolved anisotropy of the tryptophan fluorescence was strongly dependent upon emission wavelength, and these data provided critical information concerning the origin of the large spectral changes which are observed in the TBP/DNA interaction (see Figure 13, upper). At 310 nm, the very "bluest" region of the tryptophan emission spectrum, a rotational correlation time of ≃80 ns is recovered, suggesting a very high order TBP multimer complex (a spherical

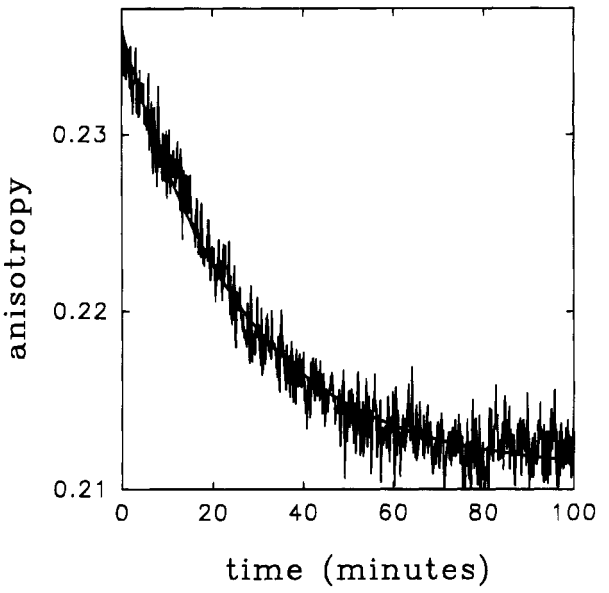

FIGURE 12: Measurement of the rate of dissociation of TBP from TATA-DNA via stopped-flow anisotropy. Off-rate stopped-flow anisotropy of prebound TBP (10 nM) with Rhodamine-X DNA (17 nM, 14mer). A time $t = 0$, 105 nM of unlabeled 18mer was rapidly mixed with the prebound complex. The off-rate of TBP from the DNA can be described using a single time constant ($1/k_{off}$) of 23 min (smooth fit through data).

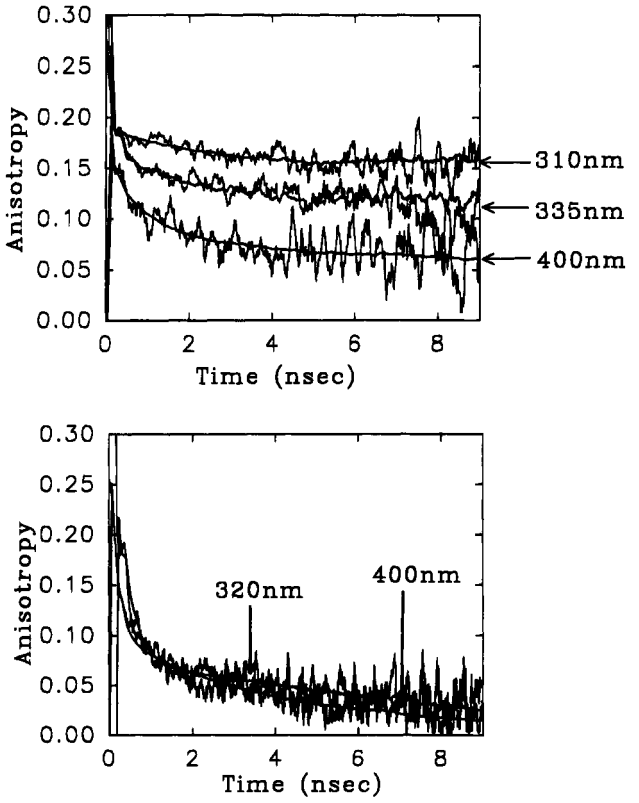

FIGURE 13: Measurement of the emission wavelength dependence of the time-resolved anisotropy of WT TBP using the single endogenous tryptophan W26. (A) Time-resolved anisotropy of free TBP excited at 295 nm and emission of 310, 335, and 400 nm. (B) Time-resolved anisotropy measurements of TBP–DNA complex at 320 and 400 nm (intermediate wavelengths also superimpose).

monomer TBP would be predicted to have a rotational correlation time of approximately 8–12 ns). At 400nm, the anisotropy decay collapses at a much faster rate, and at this wavelength the anisotropy decay resembles the decay of the

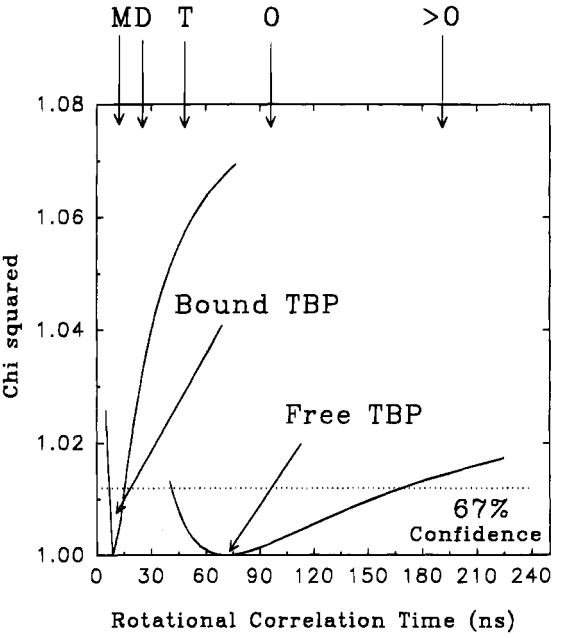

FIGURE 14: Rigorous confidence analysis of the time-resolved anisotropy decay of WT TBP when measured at 310 nm. Analysis of the rotational correlation time associated with the DNA–TBP complex data analysis yields 8.5 ± 2 ns at 67% confidence. The recovered rotational correlation time of free TBP in solution is consistent with a range of correlation times, from approximately 40 to 160 ns at 67% confidence level. Upper symbols represent approximate correlation times for spherical TBP in monomer (M), dimer (D), tetramer (T), or octamer (O) oligomeric states.

DNA-bound complex (Figure 13, lower). The anisotropy decays of the TBP–DNA bound complex are identical at each wavelength and give a rotational correlation time of ≃8.5 ns. Figure 14 illustrates rigorous confidence intervals (Beechem, 1992) for the recovered rotational correlation times when observed at 310 nm emission. The observed time-resolved anisotropy at 310 nm is consistent with a range of rotational correlation times between 40 and 165 ns. This result is consistent with the properties predicted for oligomeric forms of TBP in the tetramer–octomer range (or even somewhat larger). The rotational properties of the TBP–DNA complex are much better defined and have limits of 8.5 ± 2 ns.

Time-resolved tryptophan fluorescence decay experiments as a function of emission wavelength (decay associated spectra; DAS) allow the decomposition of the steady-state emission spectra into underlying time-resolved components (Brochon et al., 1977; Knutson et al., 1982). In this manner, additional information concerning the nature of the spectral changes upon DNA binding can be examined. Single-curve analysis of the time-resolved total-intensity data obtained at 340 nm in the absence of DNA yields three exponential lifetime terms of 0.44, 1.5, and 4.4 ns. Full global analysis of the entire time-resolved/emission wavelength data surface is shown in Figure 15. Although these DAS profiles clearly reveal dramatic red-shifts associated with DNA binding, these analyses do not in and of themselves yield much information concerning the physical nature of the emitting species. These data do reveal, however, that there are no significant lifetime/rotational correlation time association effects for the TBP–DNA bound complex (Ludescher et al., 1987).

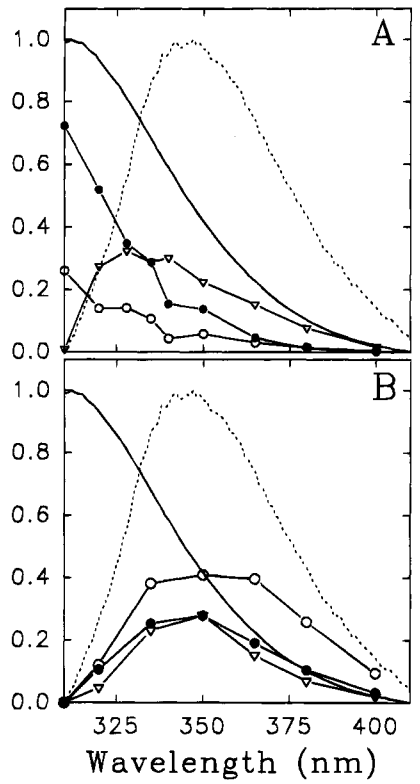

FIGURE 15: Decomposition of the observed steady-state fluorescence emission spectra of W26 in WT TBP both free in solution (solid line) and bound to TATA-DNA (dashed line) into underlying time-resolved decay associated spectra (DAS). Free TBP (A, upper) shows three DAS associated with lifetimes of ○ = 0.40 ns, ● = 1.65 ns, and ▽ = 3.8 ns. DNA-bound TBP (B, lower) shows three DAS associated with lifetimes of ○ = 0.20 ns, ● = 1.52 ns, ▽ = 5.7 ns. The protein concentration was 2 μM.

DISCUSSION

Native TBP in solution has a very blue-shifted emission spectrum, indicative of a very hydrophobic environment near W26 of the amino terminal domain. The striking red-shift in the steady-state emission spectra of this tryptophan upon binding DNA (λ_{max} 310 nm → 353 nm) reveals similarities with the changes observed upon either thermal or GuHCl denaturation (Figures 1, 4, and 5). Regardless of the physical origin of the tryptophan transition, the red-shift in the emission spectra can be used as an intrinsic spectroscopic marker for DNA binding, as shown in Figures 1−3. Binding isotherms examined at these high concentrations do not yield accurate K_d's but are very good at obtaining absolute stoichiometries and performing active-site titrations. For this reason, absolute TBP protein concentrations were determined using amino acid analysis. This allowed us to unequivocally determine that the TBP/DNA binding stoichiometry was 1:1 (see inset of Figure 2) and that our TBP protein preparations were >95% active.

It was also found that the limited proteolysis procedure, which selectively clips residues 1−40 away from the carboxy terminal domain, produced a spectral shift in W26-TBP tryptophan fluorescence identical to that induced by DNA binding, with a kinetic rate proportional to chymotrypsin concentration (data not shown). The simplest interpretation of these results is that the carboxy terminal domain of TBP is providing the hydrophobic environment for the amino terminal domain. It is also clear, however, that the higher oligimeric TBP states are more blue-shifted, suggesting that the amino terminal domain ↔ carboxy terminal domain interaction may be between *different* TBP monomers. When TBP (27 kDa) binds to duplex DNA of similar size (41mer), the molecular weight doubles and thus the TBP−DNA complex should rotate more slowly (Figure 7). However, contrary to this prediction, time-resolved tryptophan anisotropy data show a decrease in the rotational correlation time (Figure 6). The time-resolved anisotropy decay curve for the native protein detected at 350 nm emission never asymptotes down to zero. The time-resolved anisotropies of free TBP gradually decrease as a function of emission wavelength (Figure 13, upper). Time-resolved anisotropy decay observed in the 310−330 nm region, which corresponds to a more hydrophobic tryptophan environment, reveals only very slowly rotating species (i.e., higher order associated TBPs). Rigorous confidence analysis reveals a rotational correlation time of 45−165 ns (see Figure 14), which is consistent with multimeric forms of TBP as suggested originally by Nikolov et al. (1992). As one moves to longer emission wavelengths (340−410 nm), consistent with a more solvent-exposed tryptophan environment, the time-resolved anisotropy decays indicate the presence of a decreasing molecular weight species. Upon binding DNA, the emission wavelength dependence of the time-resolved anisotropy disappears. The bound TBP−DNA complex shows relatively fast motion, and it does not appear that the amino terminal domain of TBP is hydrodynamically coupled to the DNA in the bound complex, the rotational correlation time for both being 8.5 ns. These experiments reveal that native TBP free in solution is a multimeric complex with the amino terminal region(s) tucked into a hydrophobic core region. Upon binding DNA, these higher order oligomeric states of TBP are completely eliminated. Exposure of TBP to low concentrations of guanidine, or mild temperatures (above 29 °C), also caused the multimer to dissociate and the amino terminus to become more solvent exposed. It should be emphasized that even "rough-handling" of the TBP (e.g., quick thawing, repeated freeze/thaw cycles, etc.) can significantly alter the oligimerization state of the TBP. One possible physical model which is consistent with all of these spectroscopic data is shown in Figure 16. This schematic represents TBP in solution as a distribution of multimer species. The higher molecular weight complex contributes to the shorter wavelength edge of the TBP emission spectrum, while the monomeric species has a greater contribution at longer emission wavelengths. Upon DNA binding, TBP dissociates into a monomeric form. This model also illustrates the amino terminus as hydrodynamically uncoupled from the carboxy terminal DNA binding domain.

Rather surprisingly, it does not appear that this oligomerization behavior actually affects the on-rate of TBP to DNA to any significant effect, since only a single second-order rate constant is needed to describe the binding data from 20 to 600 nM TBP. If the oligomerization properties of TBP were changing significantly over this concentration range, and the various oligomeric forms had different binding rates, the successful global analysis shown in Figure 9 would not have been possible. Stopped-flow experiments which were performed using the intrinsic tryptophan fluorescence, however, do reveal a slower second-order binding rate (Figure 11). One possible origin for this difference could be complications associated with the tryptophan signal being

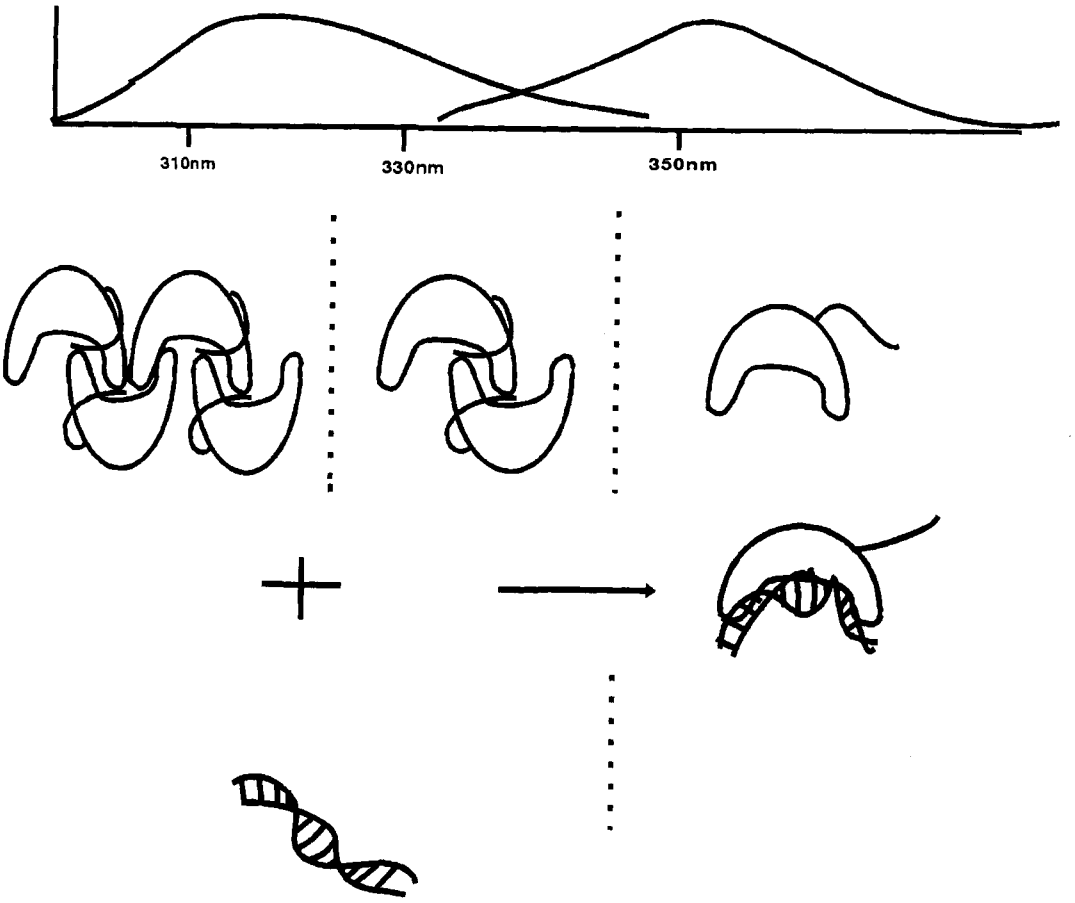

FIGURE 16: Schematic representation of the structural transitions involved in the amino terminus of multimerized TBP upon binding DNA as deduced from the changes in the intrinsic tryptophan fluorescence of WT TBP (W26). The highest association states of TBP contribute to the "bluest" emission spectra, with more monomeric states having a red-shifted spectra. Binding of TBP to DNA shifts the endogenous W26 tryptophan emission spectra to 353 nm (see text for description) and decouples (hydrodynamically) the amino terminal domain from the carboxy domain−DNA complex.

responsive primarily to the TBP oligomerization state and not the TBP−DNA bound complex . If the kinetics of TBP binding obtained by monitoring the W26 fluorophore are examined as a function of various types of "mistreatment" of the TBP, the observed binding kinetics can be dramatically changed (data not shown). For instance, the more shifted to the red the initial free TBP emission spectrum is (i.e., quick thawing TBP by hand from the freezer will cause this effect), the faster are the apparent binding kinetics to DNA. Further kinetic studies designed to directly compare the Rhodamine-X and tryptophan stopped-flow signal changes are currently in progress (Perez-Howard et al., 1995). Clearly, the changes in Rhodamine-X-labeled DNA anisotropy are much easier to interpret since the Rhodamine-X lifetime is constant ± TBP, and all of the signal change it reports are due to changes in the rotational mobility of the DNA (i.e., binding; see Figure 7). However, if the TBP/DNA interaction were purely 2-state, any spectroscopic monitor of this transition would be identical.

The Rhodamine-X-labeled TATA box DNA can be used as a very sensitive assay for TBP/DNA interaction. Similar spectroscopic assay systems have been developed for a few other systems (e.g., Heyduk & Lee, 1990; LeTilly & Royer, 1993). The high quantum yield and lifetime invariance of the Rhodamine-X probe used in this study make it possible to measure the DNA/TBP interaction at nanomolar/picomolar concentrations. Extrinsically labeled DNA measurements reveal the predicted pattern of a saturable increase in both the time-resolved and steady-state anisotropy upon interaction with TBP (e.g., Figure 7). The time-resolved anisotropy data from Rhodamine-X-labeled DNA demonstrate that the DNA "spinning" and "tumbling" modes become slower when bound by TBP. This fundamental result, itself, may be slightly surprising, since the Rhodamine-X probe is only connected to the 5′ terminus of the DNA through a very flexible $(CH_2)_6$ methylene linkage. For all of the Rhodamine-X duplex DNAs which we have examined (a variety of sizes from 12mer to 80mer), all show relatively tight coupling to changes in the rotational dynamics of the DNA. One possible mechanism for this apparent sensitivity is that the Rhodamine-X fluorophore loops-over and associates with the end of the DNA, greatly limiting the amount of local motion which the probe experiences.

Both the equilibrium and kinetic aspects of the TBP/DNA interaction have been examined using the Rhodamine-X DNA as a probe. The rate constants recovered from the stopped-flow kinetic experiments provide an independent measurement of the K_d for this system, using $K_d = k_{off}/k_{on}$. The predicted value of K_d from the stopped-flow experiments agrees very well with the equilibrium experiments (see Table 1). In fact, the uncertainty in the K_d value obtained from the kinetic data is significantly less than from the actual equilibrium experiments.

Previous kinetic studies of TBP/DNA interaction have utilized either DNase footprinting (Hahn et al., 1989a,b) or gel-shift analysis (Hoopes et al., 1992; Kuddus & Schmidt,

1993). By necessity, the data density and timing resolution of these studies were significantly less than in the present work. For instance, in previous band-shift and DNase footprinting assays, a total of 10 data points would be recorded over a time period of approximately 10 min (Hoopes et al., 1992). In this study, each kinetic trace had approximately 4000−8000 data points, with each point separated by 50 ms (although faster timing resolution was available, it was not needed for these studies). To our knowledge, this is the first reported study using stopped-flow anisotropy changes to monitor a protein/DNA kinetic interaction. The recovered second-order rate constant obtained from this study is very consistent with that obtained previously by Hawley's laboratory (Hoopes et al., 1992). The work of Kuddus et al. (1993) appears to underestimate the second-order rate constant by a factor of approximately 10. Hawley's experimental protocol utilized a vast excess of TBP over DNA, whereas Kuddus et al. utilized a large excess of DNA over TBP. In this work, a range of TBP concentrations ranging from 1:1 to 30:1 were examined. Since the differential equations describing the second-order reaction were solved numerically and directly utilized to fit all of the kinetic data, the vast excesses of reagents utilized in these previous studies were not required. All of the inherent complications associated with the enhanced off-rates of TBP in gels were also obviated. It is rather surprising that a reaction which generates such a radical change in DNA structure upon binding (Kim, J., et al., 1993; Kim, Y., et al., 1993) can be described so adequately using a simple second-order rate constant. It should be kept in mind, however, that the Rhodamine-X anisotropy signal will be dominated by changes in the rotational mobility of the DNA. Hence, additional reaction steps (e.g., "conformational" changes in the DNA which do not lead to major changes in DNA mobility) could be occurring and not be detected by these stopped-flow experiments. Although our second-order rate constant agrees completely with that of Hawley's laboratory (Hoopes et al., 1992), this group proposed a faster diffusion limited step of TBP/DNA interaction prior to the observed second-order process. However, on the basis of our results, we find absolutely no evidence of a faster, diffusion limited step in the TBP/DNA interaction kinetics.

The ΔN TBP on-rate kinetics reveal a much slower rate (45-fold slower) of binding of ΔN TBP to DNA. Further, this binding reaction does not appear to follow simple second-order kinetics. We have not completely characterized this mutant in a manner similar to the WT TBP. Absolute protein concentrations have not been determined using amino acid analysis (as we did with WT); however, it is very doubtful that the absolute concentrations of ΔN TBP are off by more than 50%, certainly by much less than a factor of 45. In addition, we know that full changes in the anisotropy function were observed under these stopped-flow conditions, indicating that the maximum that the *active* protein concentration could be in error is by a factor of 2. Therefore, it does appear that the amino terminal domain of TBP, although clearly not required in vivo, significantly increases the rate at which WT TBP can interact with TATA box DNA. The mechanism of this enhancement is unknown, although one possible suggestion would be that the predominately negatively charged amino terminal domain actually "steers" the carboxy terminal domain into the correct configuration in which to interact with the DNA.

ACKNOWLEDGMENT

We thank Roberta A. Knittle for technical assistance with polyacrylamide gel purification of the DNA oligos, for helpful advice on the handling of sensitive DNA preps, and for knowledgeable expertise and support on the molecular biological scale; David Poon for his assistance in the early stages of this work; and Stephanie Schroeder for providing amino terminal deleted TBP.

REFERENCES

Beechem, J. M. (1992) *Methods Enzymol. 210,* 37−54.
Beechem, J., & Brand, L. (1985) *Annu. Rev. Biochem. 54,* 43−71.
Beechem, J. M., Gratton, E., Ameloot, M., Knutson, J. R., & Brand, L. (1992) In *Fluorescence Spectroscopy* (Lakowicz, J., Ed.) Vol. II, Chapter V, Plenum Publishing, New York.
Brochon, J. C., Wahl, P., Charlier, M., Maurizot, J. C., & Helene, C. (1977) *Biochem. Biophys. Res. Commun. 79,* 1261−1271.
Cavallini, B., Faus, I., Matthes, H., Chipoulet, J. M., Windsor, B., Egly, J. M., & Chambon, P. (1989) *Proc. Natl. Acad. Sci. U.S.A. 86,* 9803−9807.
Chasman, D., Flaherty, K., Sharp, P. A., & Kornberg, R. D. (1993) *Proc. Natl. Acad. Sci. U.S.A. 90,* 8174−8178.
Cormack, B. P., Strubin, M., Ponticelli, A. S., & Struhl, K. (1991) *Cell 65,* 341−348.
Davison, B. L., Egly, J. M., Mulvihill, E. R., & Chambon, P. (1983) *Nature 301,* 680−686.
Dynlacht, B. D., Hoey, T., & Tijan, R. (1991) *Cell 66,* 563−576.
Fasman, G. D. (1975) *Handbook of Biochemistry, Nucleic Acids,* 3rd ed., Vol. I, CRC Press, Boca Raton, FL.
Gill, G., & Tijan, R. (1991) *Cell 65,* 333−340.
Hahn, S., Buratowski, S., Sharp, P. A., & Guarente, L. (1989a) *Cell 58,* 1173−1181.
Hahn, S., Buratowski, S., Sharp, P. A., & Guarente, L. (1989b) *Proc. Natl. Acad. Sci. U.S.A. 86,* 5718−5722.
Hernandez, N. (1993) *Genes Dev. 7* (7b), 1291−1308.
Heyduk, T., & Lee, J. C. (1990) *Proc. Natl. Acad. Sci. U.S.A. 87,* 1744−1748.
Hoopes, B. C., Le Blanc, J., & Hawley, D. (1992) *J. Biol. Chem. 267,* 11539−11547.
Horikoshi, M., Wang, C. K., Fujii, H., Cromlish, J. A., Weil, P. A., & Roeder, R. G. (1989a) *Nature 341,* 299−303.
Horikoshi, M., Wang, C. K., Fuji, H., Cromlish, J. A., Weil, P. A., & Roeder, R. G. (1989b) *Proc. Natl. Acad. Sci. U.S.A. 86,* 4843−4847.
Horikoshi, M., Yamamoto, T., Ohkuma, Y., Weil, P. A., & Roeder, R. G. (1990) *Cell 61,* 1171−1178.
Kato, K., Makino, Y., Kishimoto, T., Yamauchi, J., Kato, S., Muramatsu, M., & Tamura, T. (1994) *Nucleic Acids Res. 22,* 1179−1185.
Kelleher, R. J., Flanagan, P. M., Chasman, D. I., Ponticelli, A. S., Struhl, K., & Kornberg, A. R. (1992) *Genes Dev. 6,* 296−303.
Kim, J., Nikolov, D., & Burley, S. K. (1993) *Nature 365,* 520−527.
Kim,Y., Geiger, J., Hahn, S., & Sigler, P. B. (1993) *Nature 365,* 512−520.
Knutson, J. R., Walbridge, D. W., & Brand, L. (1982) *Biochemistry 21,* 4671−4679.
Kuddus, R., & Schmidt, M. C. (1993) *Nucleic Acids Res. 21,* 1789−1796.
Lee, D. K., Dejong, J., Hashimota, S., Horikoshi, M., & Roeder R. G. (1992) *Mol. Cell. Biol. 12,* 5189−5196.
LeTilly, V., & Royer, C. A. (1993) *Biochemistry 32,* 7753−7758.
Lieberman, P. M., Schmidt, M. C., Kao, C. C., & Berk, A. J. (1991) *Mol. Cell. Biol. 11,* 63−74.
Ludescher, R. D., Peting, L., Hudson, S., & Hudson, B. (1987) *Biophys. Chem. 28,* 59−75.
Nakajima, N., Horikoshi, M., & Roeder, R. G. (1988) *Mol. Cell. Biol. 8,* 4028−4040.
Nikolov, D. B., Hu, S. H., Lin, J., Gasch, A., Hoffman, A., Chua, N. H., Roeder, R. G., & Burley, S. K. (1992) *Nature 360,* 40−46.
Otto, M. R., Lillo, M. P., Beechem, J. M. (1994) *Biophys. J. 67,* 2511−2521.

Perez-Howard, G. M., Weil, P. A., & Beechem, J. M. (1995) *Protein Society, Ninth Symposium*, Boston, MA.

Poon, D., Schroeder, S., Wang, C. K., Yamamoto, T., Horikoshi, M., Roeder, R. G., & Weil, P. A. (1991) *Mol. Cell. Biol. 11*, 4809−4821.

Poon, D., Knittle, R. A., Sabelko, K. A., Yamamoto, T., Horikoshi, M., Roeder, R. G., & Weil, P. A. (1993) *J. Biol. Chem. 268*, 5005−5013.

Pugh, F. B., & Tijan, R. (1992) *J. Biol. Chem. 267*, 679−682.

Reddy, P., & Hahn, S. (1991) *Cell 65*, 349−357.

Schmidt, M. C., Kao, C. C., Pei, R., & Berk, A. J. (1989) *Proc. Natl. Acad. Sci. U.S.A. 86*, 7785−7789.

Tijan, R., & Maniatis, T. (1994) *Cell 77*, 5−8.

Tirado, M. M., & Garcia de la Torre, J. (1980) *J. Chem. Phys. 73*, 1986.

Van Dyke, M. W., Roeder, R. G., & Sawadogo, M. (1988) *Science 241*, 1335−1338.

Van Dyke, M. W., Sawadogo, M., & Roeder, R. G. (1989) *Mol. Cell. Biol. 9*, 342−244.

Weber, G. (1992) *Protein Interactions*, Routledge, Chapman & Hall, New York.

Zawel, L., & Reinberg, D. (1993) *Prog. Nucleic Acid Res. Mol. Biol. 44*, 67−108.

Zhou, Q., & Berk, A. J. (1995) *Mol. Cell. Biol. 15*, 534−539.

Zhou, Q., Schmidt, M. C., & Berk, A. J. (1991) *EMBO J. 10*, 1843−1852.

BI9505225